Growth factor and galaxy bias from future redshift surveys: a study on parametrizations

Cinzia Di Porto[1,2], Luca Amendola[2], Enzo Branchini[1]
[1] *Dipartimento di Fisica "E. Amaldi", Università degli Studi "Roma Tre", via della Vasca Navale 84, 00146, Roma, Italy and*
[2] *Institut für Theoretische Physik, Universität Heidelberg, Philosophenweg 16, 69120 Heidelberg, Germany and INAF/Roma*

Many experiments in the near future will test dark energy through its effects on the linear growth of matter perturbations. In this paper we discuss the constraints that future large-scale redshift surveys can put on three different parameterizations of the linear growth factor and how these constraints will help ruling out different classes of dark energy and modified gravity models. We show that a scale-independent bias can be estimated to a few percent per redshift slice by combining redshift distortions with power spectrum amplitude, without the need of an external estimation. We find that the growth rate can be constrained to within 2-4% for each $\Delta z = 0.2$ redshift slice, while the equation of state w and the index γ can be simultaneously estimated both to within 0.02. We also find that a constant dimensionless coupling between dark energy and dark matter can be constrained to be smaller than 0.14.

I. INTRODUCTION

The linear growth rate of matter perturbations is one of the most interesting observable quantities since it allows to explore the dynamical features related to the build-up of cosmic structures beyond the background expansion. For example it can be used to discriminate between cosmological models based on Einstein's gravity and alternative models like $f(R)$ modifications of gravity (see e.g. [1]) or multi-dimensional scenarios like in the Dvali-Gabadaze-Porrati (DGP) [2] theory (e.g. [3] and references therein). In addition, the growth rate is sensitive to dark energy clustering or to dark energy-dark matter interaction. For instance, in models with scalar-tensor couplings or in $f(R)$ theories the growth rate at early epochs can be larger than in ΛCDM models and can acquire a scale dependence [4–6] (see for instance [7] for a review on dark energy).

Simultaneous information on geometry and growth rate can be obtained by measuring the galaxy power spectrum or the 2-point correlation function and their anisotropies observed in redshift space. These redshift distortions arise from peculiar velocities that contribute, together with the recession velocities, to the observed redshift. The net effect is to induce a radial anisotropy in galaxy clustering that can be measured from standard two-point statistics like the power spectrum or the correlation function [8]. The amplitude of the anisotropy is determined by the typical amplitude of peculiar velocities which, in linear theory, is set by the growth rate of perturbations[1]:

$$s \equiv \frac{d\log G}{d\log a}\,, \tag{1}$$

where $G(z) \equiv \delta(z)/\delta(0)$ is the growth function, $\delta(z)$ the matter density contrast and the scale factor a is related to the redshift z through $a = (1+z)^{-1}$. Since however we only observe the clustering of galaxies and not that of the matter, the quantity that is accessible to observations is actually

$$\beta \equiv \frac{s}{b}\,, \tag{2}$$

where the bias b is the ratio of density fluctuations in galaxies and matter. The bias is in general a function of redshift and scale, but in the following we will consider it as a simple scale-independent function.

Once the power spectrum is computed in k-space, the analysis proposed in [9] can be exploited to constrain not only geometry but also the growth rate (as pointed out in [10]; see also [3, 11]), provided

[1] In order to avoid confusion with the $f(R)$ models, we use the letter s, for slope, rather than the more popular f, to indicate the growth rate.

that the power spectrum is not marginalized over its amplitude. In configuration space, the first analysis of the two-point correlation function explicitly aimed at discriminating models of modified gravity from the standard ΛCDM scenario has been performed by [12]. Currently, there are several experimental estimates of the growth factor derived from the analysis of the redshift space distortions [12–19], from the redshift evolution of the *rms* mass fluctuation σ_8 inferred from Lyα absorbers [20] and from the power spectrum of density fluctuations measured from galaxies' peculiar velocities [21]. Current uncertainties are still too large to allow these measurements to discriminate among alternative cosmological scenarios. (e.g. [22, 23]).

On-going redshift surveys like VIPERS [24] or BOSS [25] will certainly provide more stringent constraint and will be able to test those models that deviate most from the standard cosmological model. However, only next generation large-scale redshift surveys at $z \approx 1$ and beyond like EUCLID [26] or BigBOSS [27] will provide an efficient way to discriminate competing dark energy models.

The growth rate s clearly depends on the cosmological model. It has been found in several works [28–32] that a simple yet effective parameterization of s captures the behavior of a large class of models. Putting

$$s = \Omega_m^\gamma \,, \tag{3}$$

where $\Omega_m(z)$ is the matter density in units of the critical density as a function of redshift, a value $\gamma \approx 0.545$ reproduces well the ΛCDM behavior while departures from this value characterize different models. For instance the DGP is well approximated by $\gamma \approx 0.68$ [33, 34] while viable models of $f(R)$ are approximated by $\gamma \approx 0.4$ for small scales and small redshifts [5, 6]. This simple parameterization is however not flexible enough to accommodate all cases. A constant γ cannot for instance reproduce a growth rate larger than $s = 1$ in the past (as we have in $f(R)$ and scalar-tensor models) allowing at the same time $s < 1$ at the present epoch if $\Omega_m \leq 1$. Even in standard cases, a better approximation requires a slowly-varying, but not strictly constant, γ.

In addition, the measures of the growth factor obtained from redshift distortions require an estimate of the galaxy bias, which can be obtained either independently, using higher order statistics (e.g. [19, 35]) or inversion techniques [36], or self consistently, by assuming some reasonable form for the bias function *a priori* (for instance, that the bias is independent of scale, as we will assume here).

The goal of this paper is to forecast the constraints that future observations can put on the growth rate. In particular we use representative assumptions for the parameters of the EUCLID survey to provide a baseline for future experiments and we focus on the following issues. *i*) We assess how well one can constrain the bias function from the analysis of the power spectrum itself and evaluate the impact that treating bias as a free parameter has on the estimates of the growth factor. We compare the results with those obtained under the more popular approach of fixing the bias factor (and its error) to some independently-determined value. *ii*) We estimate how errors depend on the parameterization of the growth factor and on the number and type of degrees of freedom in the analysis. *iii*) We explicitly explore the case of coupling between dark energy and dark matter and assess the ability of measuring the coupling constant.

We do this in the context of the Fisher Matrix analysis. This is a common approach that has been adopted in several recent works, some of which exploring the case of a EUCLID-like survey as we do. We want to stress here that this work is, in fact, complementary to those of the other authors. Unlike most of these works, here we do not try to optimize the parameter of the EUCLID survey in order to improve the constraints on the relevant parameters, as in [37]. Instead, we adopt a representative sets of parameters that describe the survey and derive the expected errors on the interesting quantities. In addition, unlike [38] and [39], we do not explicitly aim to study the correlation between the parameters that describe the geometry of the system and the growth parameters, although in our approach we also take into account the degeneracy between geometry and growth. Finally, the main results of this paper are largely complementary to the work of [40] that perform a more systematic error analysis that does not cover the main issues of our work.

Although, as we mentioned, in general s might depend on scale, we limit this paper to an exploration of time-dependent functions only. Forecasts for specific forms of scale-dependent growth factor motivated by scalar-tensor models are in progress and will be presented elsewhere.

The layout of the paper is as follows. In the next section we will introduce the different parameterizations adopted for the growth rate and for the equation of state of dark energy, together with the models assumed for the biasing function, and describe the different cosmological models we aim to discriminate. In sec. III we will briefly review the Fisher matrix method for the power spectrum and define the adopted

fiducial model. In sec. IV we will describe the characteristics of the galaxy surveys considered in this work, while in sec. V we will report our results on the forecast errors on the parameters of interest. Finally, in sec. VI we will draw our conclusions and discuss the results.

II. MODELS

The main scope of this work is to quantify the ability of future redshift surveys to constrain the growth rate of density fluctuations. In particular we want to quantify how this ability depends on the parameterization assumed for s and for the equation of state of the dark energy w and on the biasing parameter. For this reason we explore different scenarios detailed below.

A. Equation of state

- *w-parameterization.* In order to represent the evolution of the equation of state parameter w, we use the popular CPL parameterization [41, 42]

$$w(z) = w_0 + w_1 \frac{z}{1+z} \, . \tag{4}$$

  As a special case we will also consider the case of a constant w.

B. Growth Rate

As anticipated, in this work we assume that the growth rate, s, is a function of time but not of scale. Here we explore three different parameterizations of s:

- *s-parameterization.* This is in fact a non-parametric model in which the growth rate itself is modeled as a step-wise function $s(z) = s_i$, specified in different redshift bins. The errors are derived on s_i in each i-th redshift bin of the survey.

- *γ-parameterization.* As a second case we assume

$$s \equiv \Omega_m(z)^{\gamma(z)} \, . \tag{5}$$

  where the $\gamma(z)$ function is parametrized as

$$\gamma(z) = \gamma_0 + \gamma_1 \frac{z}{1+z} \, . \tag{6}$$

  As shown by [43, 44], this parameterization is more accurate than that of eq. (3) for both ΛCDM and DGP models. Furthermore, this parameterization is especially effective to distinguish between a wCDM model (i.e. a dark energy model with a constant equation of state) that has a negative γ_1 ($-0.020 \lesssim \gamma_1 \lesssim -0.016$, for a present matter density $0.20 \leq \Omega_{m,0} \leq 0.35$) and a DGP model that instead, has a positive γ_1 ($0.035 < \gamma_1 < 0.042$). In addition, modified gravity models show a strongly evolving $\gamma(z)$ [5, 43, 45], in contrast with conventional Dark Energy models. As a special case we also consider $\gamma =$ constant (only when w also is assumed constant), to compare our results with those of previous works.

- *η-parameterization.* To explore models in which perturbations grow faster than in the ΛCDM case, like in the case of a coupling between dark energy and dark matter [4], we consider a model in which γ is constant and the growth rate varies as

$$s \equiv \Omega_m(z)^{\gamma}(1+\eta) \, , \tag{7}$$

  where η quantifies the strength of the coupling. The example of the coupled quintessence model worked out by [4] illustrates this point. In that model, the numerical solution for the growth rate can be fitted by the formula (7), with $\eta = c\beta_c^2$, where β_c is the dark energy-dark matter coupling constant and best fit values $\gamma = 0.56$ and $c = 2.1$. In this simple case, observational constraints over η can be readily transformed into constraints over β_c.

C. Galaxy Biasing

In the analysis of the redshift distortions, $s(z)$ is degenerate with the bias function $b(z)$. In absence of a well-established theory of galaxy formation and evolution, most analysis assume some arbitrary functional form for $b(z)$. However, biasing needs to be neither deterministic nor linear. Stochasticity in galaxy biasing is supposed to have little impact on two-point statistics, at least on scales significantly larger than those involved with galaxy evolution processes [46]. On the other hand, deviations from linearity (which imply scale dependency) might not be negligible. Current observational constraints based on self consistent biasing estimators [19, 36] show that nonlinear effects are of the order of a few to ~ 10 %, depending on the scale and the galaxy type [35, 47]. To account for current uncertainties in both modeling and measuring galaxy bias we consider the following choices for the functional form of b:

- *Redshift dependent bias.* We assume $b(z) = \sqrt{1+z}$ (already used in [48]) since this function provides a good fit to H_α line galaxies with luminosity $L_{H_\alpha} = 10^{42}$ erg^{-1} s^{-1} h^{-2} modeled by [49] using the semi-analytic *GALFORM* models of [50]. We consider H_α line objects since they will likely constitute the bulk of galaxies in the next generation slitless spectroscopic surveys like EUCLID. This H_α luminosity roughly corresponding, at $z = 1.5$, to a limiting flux of $f_{H\alpha} \geq 4 \times 10^{-16}$ erg cm^{-2}s^{-1}.
- *Constant bias.* For the sake of comparison, we will also consider the case of constant $b = 1$ corresponding to the rather unphysical case of a redshift-independent population of unbiased mass tracers.

D. Reference Cosmological Models

As it will be better explained in the next section, to perform the Fisher Matrix analysis we need to adopt a fiducial cosmological model. We choose the one recommended by the Dark Energy Task Force (DETF) [51]. In this "pseudo" ΛCDM model the growth rate values are obtained from eq. (3) with $\gamma = 0.545$ and $\Omega_m(z)$ is given by the standard evolution

$$\Omega_m(z) = \Omega_{m,0}(1+z)^3 \frac{H_0^2}{H(z)^2}\,, \tag{8}$$

where (the subscript 0 will generally denotes the present value)

$$H(z)^2 = H_0^2 \left[\Omega_{m,0}(1+z)^3 + \Omega_k(1+z)^2 + (1-\Omega_{m,0}-\Omega_k)\exp\left\{3\int\left(1+w_0+w_1\frac{z}{1+z}\right)\frac{dz}{1+z}\right\}\right]\,. \tag{9}$$

Then $\Omega_m(z)$ is completely specified by setting $\Omega_{m,0} = 0.25$, $\Omega_k = 0$, $w_0 = -0.95$, $w_1 = 0$. We wish to stress that regardless of the parameterization adopted, our fiducial cosmology is always chosen as the DETF one. In particular we choose as fiducial values $\gamma_1 = 0$ and $\eta = 0$, when the corresponding parameterizations are employed.

One of the goals of this work is to assess whether the analysis of the power spectrum in redshift-space can distinguish the fiducial model from alternative cosmologies, characterized by their own set of parameters (apart from $\Omega_{m,0}$ which is set equal to 0.25 for all of them). The alternative models that we consider in this work are:

- *DGP model.* We consider the flat space case studied in [52]. When we adopt this model then we set $\gamma_0 = 0.663, \gamma_1 = 0.041$ [43] or $\gamma = 0.68$ [33] and $w = -0.8$ when γ and w are assumed constant.
- *$f(R)$ model.* Here we consider the one proposed in [53], depending on two parameters, n and λ, which we fix to $n = 2$ and $\lambda = 3$. In this case we assume $\gamma_0 = 0.43$, $\gamma_1 = -0.2$, values that apply quite generally in the limit of small scales (provided they are still linear, see [5]) or $\gamma = 0.4$ and $w = -0.99$.
- *coupled dark energy (CDE) model.* This is the coupled model proposed by [54, 55]. In this case we assume $\gamma_0 = 0.56$, $\eta = 0.056$ (this value comes from putting $\beta_c = 0.16$ as coupling, which is of the order of the maximal value allowed by CMB constraints) [56]. As already explained, this model cannot be reproduced by a constant γ.

III. FISHER MATRIX ANALYSIS

In order to constrain the parameters, we use the Fisher matrix method [57] (see [58] for a review), that we apply to the power spectrum analysis in redshift space following [9]. For this purpose we need an analytic model of the power spectrum in redshift space as a function of the parameters that we wish to constrain. The analytic model is obtained in three steps. (*i*) First of all we compute with CMBFAST [59] the linear power spectrum of the matter in real space at $z = 0$, $P_{0r}(k)$, choosing a reference cosmology where the parameters to be given as input (i.e. $\Omega_{m,0}h^2$, $\Omega_{b,0}h^2$, h, n_s also employed in the Fisher matrix analysis, plus the other standard parameters required by the CMBFAST code) are set to the values given in the III column of Tab. I while for the normalization of the spectrum we use $\sigma_8 = 0.8$. (*ii*) Second, we model the linear redshift-space distortions as

$$P_{\rm obs}(z;k,\mu) = P_{0r}(k)\frac{D_F^2(z)H(z)}{D^2(z)H_F(z)}G^2(z)b^2(z)(1+\beta(z)\mu^2)^2 + P_{\rm s}(z)\ . \tag{10}$$

Here the subscript F indicates quantities evaluated on the fiducial model. In this expression $H(z)$ is the expansion history in Eq. 9, $D(z)$ is the angular diameter distance, $G(z)$ the growth factor and $P_s(z)$ represents a scale-independent offset due to imperfect removal of shot-noise. Finally $\beta(z)$ is the redshift distortion parameter and the term $(1+\beta\mu^2)^2$ is the factor invoked by [60] to account for linear distortion in the distant-observer's approximation, where μ is the direction cosine of the wavenumber $\boldsymbol{k}$ with respect to the line of sight. As shown in [10, 11] and recently in [37], the inclusion of growth rate information reduces substantially the errors on the parameters, improving the figure of merits. (*iii*) As a third and final step we account for nonlinear effects. On scales larger than ($\sim 100\,h^{-1}$Mpc) where we focus our analysis, nonlinear effects can be represented as a displacement field in Lagrangian space modeled by an elliptical Gaussian function. Therefore, following [61, 62], to model nonlinear effect we multiply $P_{0r}(k)$ by the factor

$$\exp\left\{-k^2\left[\frac{(1-\mu^2)\Sigma_\perp^2}{2} + \frac{\mu^2\Sigma_\parallel^2}{2}\right]\right\}\ , \tag{11}$$

where $\Sigma_\perp$ and $\Sigma_\parallel$ represent the displacement across and along the line of sight, respectively. They are related to the growth factor G and to the growth rate s through $\Sigma_\perp = \Sigma_0 G$ and $\Sigma_\parallel = \Sigma_0 G(1+s)$. The value of Σ_0 is proportional to σ_8. For our reference cosmology where $\sigma_8 = 0.8$ [63], we have $\Sigma_0 = 11\,h^{-1}$Mpc.

The observed power spectrum in a given redshift bin depends therefore on a number of parameters, denoted collectively as p_i, such as the Hubble constant at present h, the reduced matter and baryon fractions at present, $\Omega_{m,0}h^2$ and $\Omega_{b,0}h^2$, the curvature density parameter Ω_k, the spectral tilt n_s plus the parameters that enter in the parameterizations described in the previous section: w_0, w_1 (or simply w); γ_0, γ_1 (or γ) and η. They are listed in Tab. I and are referred to as "Cosmological parameters". These parameters will be left free to vary while we always fix σ_8=0.8 since the overall amplitude is degenerate with growth rate and bias. The other free parameters depend on the redshift. They are listed in the lower part of Tab. I and include the expansion history $H(z)$, the growth factor $G(z)$, the angular diameter distance $D(z)$, the shot noise $P_s(z)$, the growth rate $s(z)$, the redshift distortion parameter $\beta(z)$ and the galaxy bias $b(z)$.

Given the model power spectrum we calculate, numerically or analytically, the derivatives

$$\left(\frac{\partial \ln P_{\rm obs}}{\partial p_i}\right)_F\ , \tag{12}$$

evaluated at the parameter values of the fiducial model and we obtain for the i-th redshift bin all the elements of the Fisher matrix through [64]

$$F_{ij} = \frac{1}{8\pi^2}\int_{-1}^{+1} d\mu \int_{k_{\rm min}}^{k_{\rm max}} dk\ k^2 \left(\frac{\partial \ln P_{\rm obs}}{\partial p_i}\frac{\partial \ln P_{\rm obs}}{\partial p_j}\right)_F V_{\rm eff}(k,\mu)\exp[-k^2\Sigma_\perp^2 - k^2\mu^2(\Sigma_\parallel^2 - \Sigma_\perp^2)]\,, \tag{13}$$

where

$$V_{\rm eff}(k,\mu) = \left[\frac{nP(k,\mu)}{nP(k,\mu)+1}\right]^2 V_{\rm survey}\,, \tag{14}$$

is the effective volume of the survey sampled at the scale k along the direction μ. $V_{\rm survey}$ and n represent the volume of the survey and the mean number density of galaxies in each redshift bin.

As a fiducial model we assume a "pseudo" ΛCDM with $w_0 = -0.95$; the differences with the standard $w_0 = -1.0$ ΛCDM model are rather small. For example, in the case of the γ-*parameterization*, our fiducial model has $\gamma_0 = 0.545$, $\gamma_1 = 0$ whereas the standard ΛCDM model has $\gamma_0 = 0.556$, $\gamma_1 - 0.018$ [43]. To summarize, our fiducial model is the same model recommended by the Dark Energy Task Force [51], i.e.: $\Omega^F_{m,0} = 0.25$, $\Omega^F_{b,0} = 0.0445$, $\Omega^F_k = 0$, $h^F = 0.7$, $n^F_s = 1$, $w^F_0 = -0.95$, $w^F_1 = 0$, $\gamma^F = 0.545$, $P^F_s = 0$. In addition, we assume that $\gamma^F_1 = 0$, $\eta^F = 0$. The fiducial values for the redshift dependent parameters are computed in every bin through the standard Friedmann-Robertson-Walker relations

$$\frac{H^F(z)}{100h^F} = \left[\Omega^F_{m,0}(1+z)^3 + (1-\Omega^F_{m,0})(1+z)^{3(1+w^F_0)}\right]^{1/2} , \tag{15}$$

$$D^F(z) = (1+z)^{-1}\int_0^z \frac{dz'}{H^F(z')} , \tag{16}$$

$$s^F(z) = \Omega^F_m(z)\gamma^F , \tag{17}$$

$$G^F(z) = \exp\left\{\int_0^z s^F(z)\frac{dz}{1+z}\right\} , \tag{18}$$

$$\beta^F(z) = \frac{\Omega^F_m(z)^{\gamma^F}}{b^F(z)} , \tag{19}$$

$$b^F(z) = 1 \quad \text{or} \quad b^F(z) = \sqrt{1+z} , \tag{20}$$

$$P^F_s(z) = 0 . \tag{21}$$

At this point our analysis is performed in two ways, according to the choice of z-dependent parameters that characterize the power spectrum:

- *Internal bias method.*

  We assume some fiducial form for $b(z)$ (z-dependent or constant) and express the growth function $G(z)$ and the redshift distortion parameter $\beta(z)$ in terms of the growth rate s (see eqs. (22), (2)). When we compute the derivatives of the spectrum (eq. (12)), $b(z)$ and $s(z)$ are considered as independent parameters in each redshift bin. In this way we can compute the errors on b (and s) self consistently by marginalizing over all other parameters.

- *External bias method.*

  In this case we also assume the same forms for $b(z)$ as in the *Internal bias* case but we do not explicit $G(z)$ and $\beta(z)$ in terms of s. The independent parameters are now the product $G(z)\cdot b(z)$ (if we considered them separately, the Fisher matrix would result singular) and $\beta(z)$. In this case we compute the errors over $\beta(z)$ marginalizing over all other parameters. Since we also marginalize over $(G\cdot b)^2$, in this case we cannot estimate the error over b from the Fisher matrix. Thus, in order to obtain the error over s (related to β through $s = \beta\cdot b$) with standard error propagation, we need to assume an "external" error for $b(z)$. We allow the relative error $\Delta b/b$ to be either 1% or 10%, two values that bracket the ranges of expected errors contributed by model uncertainties and deviations from linear biasing.

IV. MODELING THE REDSHIFT SURVEY

The main goals of next generation redshift surveys will be to constrain the Dark Energy parameters and to explore models alternative to standard Einstein Gravity. For these purposes they will need to consider very large volumes that encompass $z \sim 1$, i.e. the epoch at which dark energy started dominating the energy budget, spanning a range of epochs large enough to provide a sufficient leverage to discriminate among competing models at different redshifts. The additional requirement is to observe some homogeneous class of objects that are common enough to allow a dense sampling of the underlying mass density field.

Cosmological parameters in $P_{obs}(z;k,\mu)$		Fiducial values
Reduced total matter density	$\Omega_{m,0}h^2$	$0.25\cdot(0.7)^2$
Reduced baryon density	$\Omega_{b,0}h^2$	$0.0445\cdot(0.7)^2$
Curvature density	Ω_k	0
Hubble constant at present	h	0.7
Primordial fluctuation slope	n_s	1
Constant growth index	γ	0.545
γ-*parameterization* parameters	γ_0, γ_1	0.545, 0
η-*parameterization* parameters	γ, η	0.545, 0
Redshift dependent parameters		
Hubble parameter	$\log H$	eq. (15)
Angular diameter distance	$\log D$	eq. (16)
Growth rate	$\log s$	eq. (17)
Growth factor	$\log G$	eq. (18)
Redshift distortion parameter	$\log\beta$	eq. (19)
Shot noise	P_s	0
Bias	$\log b$	1, $\sqrt{1+z}$

Table I: Parameters.

As anticipated in the introduction, in this paper we consider as a reference case the spectroscopic survey proposed by the EUCLID collaboration [26]. We stress that our aim is not to focus on this particular redshift survey and assess how the constraints on the relevant parameters depends on the survey characteristics in order to optimize future observational strategies. On the contrary, under the hypothesis that next-generation space-based all-sky redshift surveys will be similar to the EUCLID spectroscopic survey, we consider the latter as a reference case and estimate how the expected errors on the bias, growth rate, coupling constant and other relevant quantities will change when one consider slightly different observational setups. For this purpose we take advantage of the huge effort made by the EUCLID team to simulate the characteristic of the target objects and compute the expected selection function and detection efficiency of the survey and adopt the same survey parameters presented in [65].

Here we consider a survey covering a large fraction of the extragalactic sky ($|b|\geq 20^\circ$), corresponding to $\sim$ 20000 deg^2 capable to measure a large number of galaxy redshifts out to $z\sim 2$. A promising observational strategy is to target H_α emitters at near-infrared wavelengths (which implies $z>0.5$) since they guarantee both relatively dense sampling (the space density of this population is expected to increase out to $z\sim 2$) and an efficient method to measure the redshift of the object. The limiting flux of the survey should be the tradeoff between the requirement of minimizing the shot noise, the contamination by other lines (chiefly among them the [O II] line), and that of maximizing the so-called efficiency ε, i.e. the fraction of successfully measured redshifts. To minimize shot noise one should obviously strive for a low flux. Indeed, the authors in [65] found that a limiting flux $f_{H\alpha}\geq 1\times10^{-16}$ erg cm^{-2}s^{-1} would be able to balance shot noise and cosmic variance out to $z=1.5$. However, simulated observations of mock H_α galaxy spectra have shown that ε ranges between 30 % and 60% (depending on the redshift) for a limiting flux $f_{H_\alpha}\geq 3\times10^{-16}$ erg cm^{-2}s^{-1} [26]. Moreover, contamination from [O II] line drops from 12% to 1% when the limiting flux increases from 1×10^{-16} to 5×10^{-16} [65]. Taking all this into account we adopt a conservative choice and consider three different surveys characterized by a limiting flux of 3, 4 and 5×10^{-16} ergcm^{-2}s^{-1}.

We use the number density of H_α galaxies at a given redshift, $n(z)$, estimated in [65] using the latest empirical data and obtained by integrating the H_α luminosity function above the minimum luminosity set by the limiting flux $L_{H_\alpha,\mathrm{min.}}=4\pi D_L(z)^2 f_{H_\alpha}$ where $D_L(z)$ is the luminosity distance. To obtain the effective number density one has to account for the success rate in measuring galaxy redshifts from H_α lines. The effective number density is then obtained by multiplying $n(z)$ by the already mentioned efficiency, ε. In the range of redshifts and fluxes considered in this work the value of ε varies in the interval [30%, 50%] (see Fig. A.1.4 of [26]).

In an attempt to bracket current uncertainties in modeling galaxy surveys, we consider the following choices for the survey parameters:

- *Reference case (ref.).* Limiting flux: $f_{H\alpha}\geq 4\times10^{-16}$ erg cm^{-2}s^{-1}, which gives the galaxy number densities listed in Col. 2 of Tab. II. The efficiency is set to $\varepsilon=0.5$.

z	$n_1(z)\times10^{-3}$	$n_2(z)\times10^{-3}$	$n_3(z)\times10^{-3}$
0.5-0.7	4.69	3.56	2.8
0.7-0.9	3.33	2.42	1.84
0.9-1.1	2.57	1.81	1.33
1.1-1.3	2.1	1.44	1.03
1.3-1.5	1.52	0.99	0.68
1.5-1.7	0.92	0.55	0.35
1.7-1.9	0.54	0.29	0.17
1.9-2.1	0.31	0.15	0.08

Table II: Expected galaxy number densities in units of $(h/\mathrm{Mpc})^3$ for EUCLID survey.

- *Optimistic case (opt.).* Limiting flux: $f_{\mathrm{H}\alpha} \geq 3\times10^{-16}$ erg cm^{-2}s^{-1}, which gives the galaxy number densities listed in Col. 1 of Tab. II. The efficiency is set to $\varepsilon = 0.5$.
- *Pessimistic case (pess.).* Limiting flux: $f_{\mathrm{H}\alpha} \geq 5\times10^{-16}$ erg cm^{-2}s^{-1}, which gives the galaxy number densities listed in Col. 3 of Tab. II. The efficiency is set to $\varepsilon = 0.3$.

The total number of observed galaxies ranges from $3\cdot10^7$ (pess.) to $9\cdot10^7$ (opt.). For all cases we assume that the relative error on the measured redshift is $\sigma_z = 0.001$, independent of the limiting flux of the survey.

V. RESULTS

In this section we present the main result of the Fisher matrix analysis that we split into two sections to stress the different emphasis given in the two approaches. We note that in all tables below we always quote errors at 68% probability level and draw in the plots the probability regions at 68% and/or 95% (denoted for shortness as 1 and 2σ values). Moreover, in all figures, all the parameters that are not shown have been marginalized over or fixed to a fiducial value when so indicated.

A. s-parameterization

This analysis has two main goals: that of figuring out our ability to estimate the biasing parameter and that of estimating the growth rate with no assumptions on its redshift dependence. The total number of parameters that enter in the Fisher matrix analysis is 45: 5 parameters that describe the background cosmology ($\Omega_{m,0}h^2, \Omega_{b,0}h^2$, h, n, Ω_k) plus 5 z-dependent parameters specified in 8 redshift bins evenly spaced in the range $z = [0.5, 2.1]$. They are $P_{\mathrm{s}}(z)$, $D(z)$, $H(z)$, $s(z)$, $b(z)$ in the *internal bias* case, while we have $\beta(z)$ and $G(z)\cdot b(z)$ in the place of $s(z)$ and $b(z)$ when we use the *external bias* method.

The subsequent analysis depends on the bias method adopted.

- In case of the *internal bias* method, the fiducial growth function $G(z)$ in the $(i+1)$-th redshift bin is evaluated from a step-wise, constant growth rate $s(z)$ as

$$G(z) = \exp\left\{\int_0^z s(z)\frac{dz}{1+z}\right\} = \prod_i \left(\frac{1+z_i}{1+z_{i-1}}\right)^{s_i}\left(\frac{1+z}{1+z_i}\right)^{s_{i+1}}. \tag{22}$$

  To obtain the errors on s_i and b_i we compute the elements of the Fisher matrix and marginalize over all other parameters. In this case one is able to obtain, self-consistently, the error on the bias and on the growth factor at different redshifts, as detailed in Tab. III and Tab. IV respectively.

  Tab. III illustrates one important result: through the analysis of the redshift-space galaxy power spectrum in a next-generation EUCLID-like survey, it will be possible to measure galaxy biasing in $\Delta z = 0.2$ redshift bins with less than 3.5% error, provided that the bias function is independent on scale. This fact can be appreciated in Fig. 1 in which we show the expected relative error as a function of redshift for both $b(z)$ functions and for the survey *Pessimistic case*. Errors are very similar in all but the outermost redshift shells. We show the *Pessimistic case* since with a more

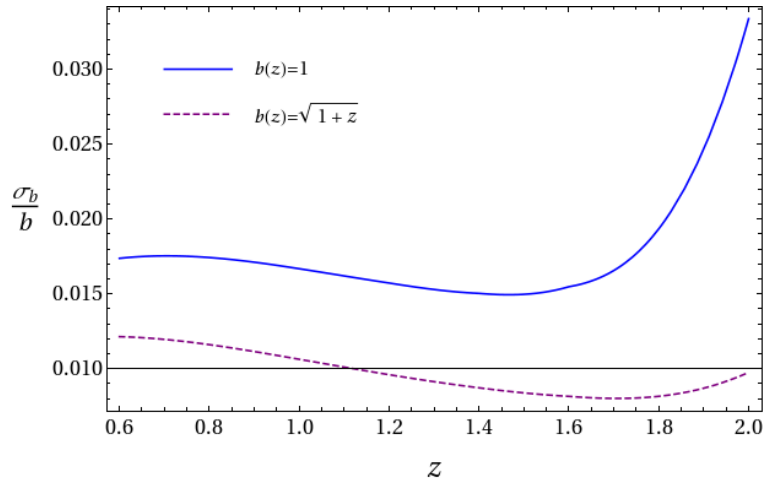

Figure 1: Relative errors over the bias parameter as a function of redshift, computed through the Fisher matrix analysis with the "internal bias" method for the *pessimistic* case. The blue solid line refers to the fiducial bias $b = 1$, while the purple dashed line refers to $b = \sqrt{1+z}$. The precision in measuring the bias has a little dependence on the $b(z)$ form: errors are very similar (the discrepancy is less than 1%) but in the outermost redshift shells (where however is less than 3%).

favorable survey configuration, like the *Reference case*, the errors would be almost identical. In addition we find that the precision in measuring the bias has a little dependence on the $b(z)$ form. The largest discrepancy between the $b(z) = 1$ and $b(z) = \sqrt{1+z}$ cases is $\sim 3\%$ and refers to the expected errors on the growth rate at $z = 2$ in the *Pessimistic case*. Differences are typically much smaller for all other parameters or, for $s(z)$ at lower redshifts or with a more favorable survey setup. Given the robustness of the results on the choice of $b(z)$ in the following we only consider the $b(z) = \sqrt{1+z}$ case.

In Fig. 2 we show the errors on the growth rate s as a function of redshift, overplotted to our fiducial ΛCDM (green solid curve). The three sets of error bars are plotted in correspondence of the 8 redshift bins and refer (from left to right) to the *Optimistic, Reference* and *Pessimistic* cases, respectively. The other curves show the expected growth rate in three alternative cosmological models: flat DGP (red dashed curve), $f(R)$ (blue dotted curve) and CDE (purple, dot-dashed curve). This plot clearly illustrates the ability of next generation surveys to distinguish between alternative models, even in the less favorable choice of survey parameters.

- In case of the *external bias* method we marginalize over the overall amplitude $(G \cdot b)^2$. Since, in this case, we cannot find errors self-consistently, we assume that bias has been determined *a priori* with errors per redshift bin of 1% and 10%, two values that should bracket the expected range of uncertainties. We note that the *external bias* method can be considered more conservative, especially in the case of large errors although we see no obvious reason why it should be preferred to the *internal bias* method that seems to provide similar results. Indeed, the errors on s relative to the 1% bias error listed in Table V are quite similar to those of the *internal bias* case. As expected, errors on s increase significantly when the bias is known with 10% accuracy rather than 1%. However, even in this case, one keeps the ability of distinguishing between most of the competing cosmological models at 1σ level, as shown in Fig. 3.

The main results of this section can be summarized as follows.

1. The ability of measuring the biasing function is not too sensitive to the characteristic of the survey ($b(z)$ can be constrained to within 1.5% in the *Optimistic* scenario and up to 3.5% in the *Pessimistic* one) provided that the bias function is independent on scale. Moreover, the precision in measuring the bias has a very little dependence on the $b(z)$ form.

2. The growth rate s can be estimated to within 1-3% in each bin for the *Reference case* survey with

$b(z)=1$ (internal)				$b(z)=\sqrt{1+z}$ (internal)		
σ_b			z	σ_b		
ref.	opt.	pess.		ref.	opt.	pess.
0.014	0.012	0.017	0.6	0.012	0.011	0.015
0.014	0.012	0.017	0.8	0.012	0.011	0.016
0.013	0.012	0.017	1.0	0.012	0.011	0.015
0.012	0.011	0.016	1.2	0.011	0.010	0.014
0.012	0.011	0.015	1.4	0.011	0.010	0.013
0.012	0.010	0.025	1.6	0.010	0.010	0.013
0.012	0.010	0.019	1.8	0.010	0.010	0.014
0.016	0.011	0.033	2.0	0.011	0.010	0.017

Table III: 1σ marginalized errors for the bias in each redshift bin obtained with the "internal bias" method.

$b(z)=1$ (internal)					$b(z)=\sqrt{1+z}$ (internal)		
σ_s			z	s^F	σ_s		
ref.	opt.	pess.			ref.	opt.	pess.
0.011	0.010	0.013	0.6	0.73	0.010	0.010	0.012
0.011	0.010	0.015	0.8	0.78	0.011	0.010	0.013
0.013	0.011	0.016	1.0	0.83	0.012	0.010	0.015
0.013	0.012	0.018	1.2	0.86	0.013	0.011	0.017
0.014	0.012	0.019	1.4	0.89	0.014	0.012	0.019
0.016	0.013	0.023	1.6	0.91	0.016	0.013	0.022
0.019	0.015	0.032	1.8	0.92	0.018	0.015	0.028
0.027	0.018	0.057	2.0	0.93	0.024	0.017	0.044

Table IV: 1σ marginalized errors for the growth rates in each redshift bin (Fig. 2) obtained with the "internal bias" method.

no need of estimating the bias function $b(z)$ from some dedicated, independent analysis using higher order statistics [19] or full-PDF analysis [36].

3. If the the bias were measured to within 1% in each slice, then the error over s would be very similar (just 1-2% larger) to that obtained by the internal estimate of $b(z)$.

4. The estimated errors on s depend weakly on the fiducial model of $b(z)$.

$b(z)=1$ (external)							$b(z)=\sqrt{1+z}$ (external)					
$\Delta b/b=1\%$			$\Delta b/b=10\%$			z	$\Delta b/b=1\%$			$\Delta b/b=10\%$		
σ_s			σ_s				σ_s			σ_s		
ref.	opt.	pess.	ref.	opt.	pess.		ref.	opt.	pess.	ref.	opt.	pess.
0.014	0.013	0.015	0.074	0.074	0.074	0.6	0.015	0.014	0.016	0.074	0.074	0.074
0.012	0.012	0.014	0.079	0.079	0.079	0.8	0.013	0.013	0.015	0.079	0.079	0.079
0.012	0.011	0.014	0.083	0.083	0.083	1.0	0.013	0.012	0.014	0.083	0.083	0.083
0.012	0.012	0.015	0.086	0.086	0.087	1.2	0.013	0.012	0.015	0.086	0.087	0.087
0.014	0.012	0.018	0.089	0.089	0.089	1.4	0.014	0.013	0.027	0.089	0.089	0.089
0.017	0.014	0.025	0.092	0.091	0.094	1.6	0.016	0.014	0.022	0.092	0.091	0.093
0.023	0.017	0.042	0.095	0.093	0.101	1.8	0.019	0.016	0.031	0.094	0.093	0.097
0.036	0.023	0.082	0.099	0.096	0.124	2.0	0.027	0.019	0.052	0.097	0.095	0.107

Table V: 1σ marginalized errors for the growth rates in each redshift bin (Fig. 3) obtained with the "external bias" method.

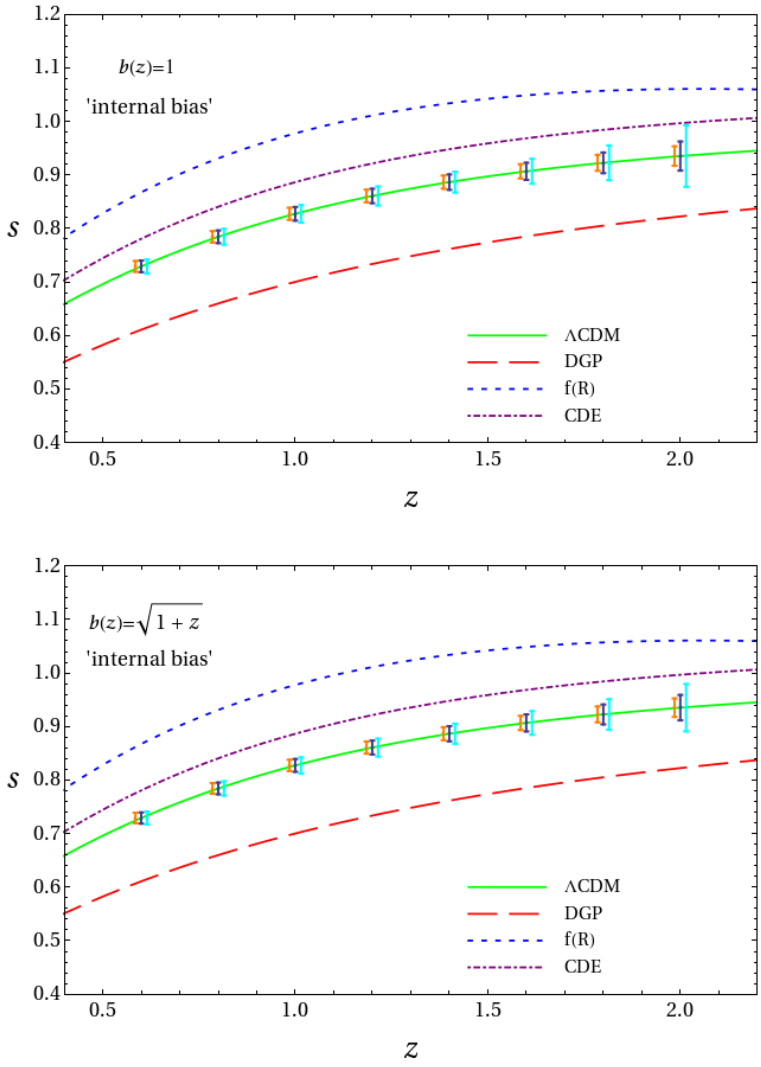

Figure 2: Expected constraints on the growth rates in each redshift bin (using the "internal bias" method). The upper panel refers to $b = 1$, while the lower panel to $b = \sqrt{1+z}$. For each z the central error bars refer to the *Reference case* while those referring to the *Optimistic* and *Pessimistic* case have been shifted by -0.015 and +0.015 respectively. The growth rates for four different models are also plotted: ΛCDM (green solid curve), flat DGP (red dashed curve), $f(R)$ model (blue dotted curve) and a model with coupling between dark energy and dark matter (purple, dot-dashed curve). In this case it will be possible to distinguish these models with next generation data.

B. Other parameterizations.

In this section we assess the ability of estimating $s(z)$ when it is expressed in one of the parametrized forms described in Section II B. More specifically, we focus on the ability of determining γ_0 and γ_1, in the context of the γ-*parameterization* and γ, η in the η-*parameterization*. In both cases the Fisher matrix elements have been estimated by expressing the growth factor as

$$G(z) \;=\; \delta_0 \exp\left[(1+\eta)\int_0^z \Omega_m(z')^{\gamma(z)}\frac{dz'}{1+z'}\right], \tag{23}$$

where for the γ-*parameterization* we fix $\eta = 0$. In this section we adopt the *internal bias* approach and assume that $b(z) = \sqrt{1+z}$ since, as we have checked, in the case of $b(z) = 1$ one obtains very similar results.

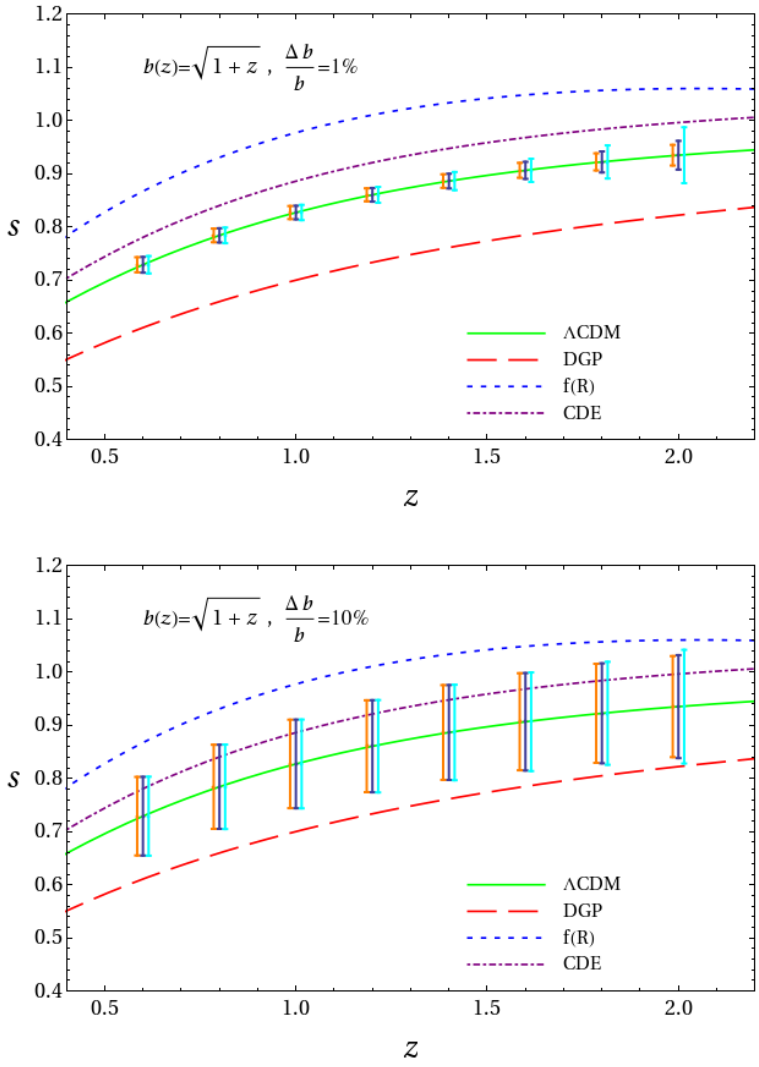

Figure 3: Expected constraints on the growth rates in each redshift bin (using the "external bias" method), assuming for the bias a relative error of 1% (upper panel) and 10% (lower panel). For each z the central error bars refer to the *Reference case* while those referring to the *Optimistic* and *Pessimistic* case have been shifted by -0.015 and +0.015 respectively. The growth rates for four different models are also plotted: ΛCDM (green solid curve), flat DGP (red dashed curve), $f(R)$ model (blue dotted curve) and a model with coupling between dark energy and dark matter (purple, dot-dashed curve). Even in the case of large errors (10%) for the bias it will be possible to distinguish among three of these models with next generation data.

- *γ-parameterization.* We start by considering the case of constant γ and w in which we set $\gamma = \gamma^F = 0.545$ and $w = w^F = -0.95$. As we will discuss in the next Section, this simple case will allow us to cross-check our results with those in the literature. In Fig. 4 we show the marginalized probability regions, at 1 and 2σ levels, for γ and w. The regions with different shades of green illustrates the *Reference case* for the survey whereas the blue long-dashed and the black short-dashed ellipses refer to the *Optimistic* and *Pessimistic* cases, respectively. Errors on γ and w are listed in Tab. VI together with the corresponding figures of merit [FOM] defined to be the squared inverse of the Fisher matrix determinant and therefore equal to the inverse of the product of the errors in the pivot point, see [51]. Contours are centered on the fiducial model. The blue triangle and the blue square represent the flat DGP and the $f(R)$ models' predictions, respectively. It is clear that, in the case of constant γ and w, the measurement of the growth rate in a EUCLID-like survey will allow us to discriminate among these models. These results have been obtained by fixing the

	case	σ_γ	σ_w	FOM
$b = \sqrt{1+z}$	ref.	0.02	0.02	2115
	opt.	0.019	0.019	2806
Ω_k fixed	pess.	0.03	0.03	1296

Table VI: Numerical values for 1σ constraints on parameters in Fig. 4 and figures of merit. Here we have fixed Ω_k to its fiducial value.

curvature to its fiducial value $\Omega_k = 0$. If instead, we consider curvature as a free parameter and marginalize over, the errors on γ and w increase significantly, as shown in Table VII, and yet the precision is good enough to distinguish the different models. For completeness, we also computed the fully marginalized errors over the other Cosmological parameters for the reference survey, given in Tab. VIII.

As a second step we considered the case in which γ and w evolve with redshift according to eqs. (6) and (4) and then we marginalize over the parameters γ_1, w_1 and Ω_k. The marginalized probability contours are shown in Fig. 5 in which we have shown the three survey setups in three different panels to avoid overcrowding. Dashed contours refer to the z-dependent parameterizations while red, continuous contours refer to the case of constant γ and w obtained after marginalizing over Ω_k. Allowing for time dependency increases the size of the confidence ellipses since the Fisher matrix analysis now accounts for the additional uncertainties in the extra-parameters γ_1 and w_1; marginalized error values are in columns $\sigma_{\gamma_{\rm marg,1}}$, $\sigma_{w_{\rm marg,1}}$ of Tab. IX. We note, however, that errors are still small enough to distinguish the fiducial model from the $f(R)$ and DGP scenarios.

We have also projected the marginalized ellipses for the parameters γ_0 and γ_1 and calculated their marginalized errors and figures of merit, which are reported in Tab. X. The corresponding uncertainties contours are shown in Fig. 6. Once again we overplot the expected values in the $f(R)$ and DGP scenarios to stress the fact that one is expected to be able to distinguish among competing models, irrespective on the survey's precise characteristics.

As a further test we have estimated how the errors on γ_0 depend on the number of parameters explicitly involved in the Fisher matrix analysis. Fig. 7 shows the expected 1σ errors on γ (Y-axis) as a function of the number of parameters that are fixed when computing the element of the Fisher matrix (the different combinations of the parameters are shown on the top of the histogram elements). We see that error estimates can decrease up to ~ 50 % when parameters are fixed to some fiducial value, or are determined independently.

- *η-parameterization.*

  We have repeated the same analysis as for the *γ-parameterization* taking into account the possibility of coupling between DE and DM i.e. we have modeled the growth factor according to eq. (7) and the dark energy equation of state as in eq. (4) and marginalized over all parameters, including Ω_k. The marginalized errors are shown in columns $\sigma_{\gamma_{\rm marg,2}}$, $\sigma_{w_{\rm marg,2}}$ of Tab. IX and the significance contours are shown in the three panels of Fig. 8 which is analogous to Fig. 5. The uncertainty ellipses are now larger than in the case of the *γ-parameterization* and show that DGP and $f(R)$ models could be rejected at $> 1\sigma$ level only if the redshift survey parameter will be more favorable than in the *Pessimistic case*.

  Marginalizing over all other parameters we can compute the uncertainties in the γ and η parameters, as listed in Tab. XI. The relative confidence ellipses are shown in the left panel of Fig. 9. This plot shows that next generation EUCLID-like surveys will be able to distinguish the reference model with no coupling (central, red dot) to the CDE model proposed by [56] (white square) only at the 1-1.5 σ level.

Finally, in order to explore the dependence on the number of parameters and to compare our results to previous works, we also draw the confidence ellipses for w_0, w_1 with three different methods: *i*) fixing γ_0, γ_1 to their fiducial values and marginalizing over all the other parameters; *ii*) marginalizing over all parameters plus γ_0, γ_1 but fixing Ω_k; *iii*) marginalizing over all parameters but w_0, w_1. As one can see in Fig. 10 and Tab. XII this progressive increase in the number of marginalized parameters reflects in a widening of the ellipses with a consequent decrease in the figures of merit. These results are in agreement with those of other authors (e.g. [37, 40]).

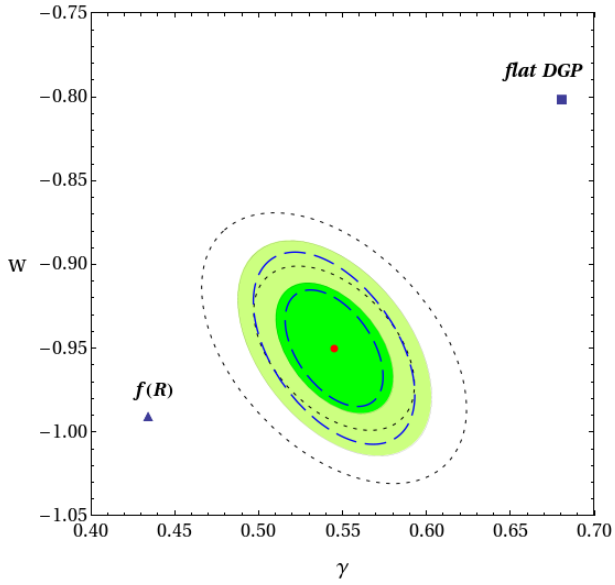

Figure 4: γ-parameterization. 1 and 2σ marginalized probability regions for constant γ and w: the green (shaded) regions are relative to the *Reference case*, the blue long-dashed ellipses to the *Optimistic case*, while the black short-dashed ellipses are the probability regions for the *Pessimistic case*. The red dot marks the fiducial model; two alternative models are also indicated for comparison.

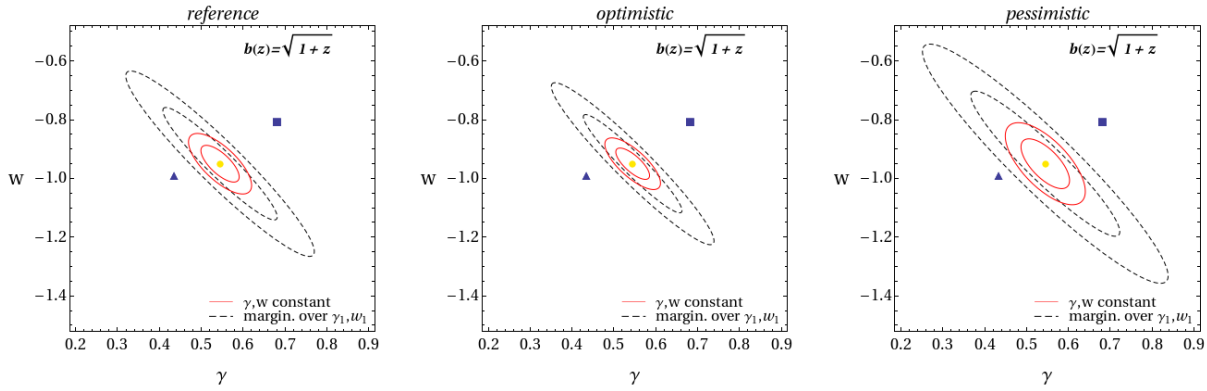

Figure 5: γ-parameterization. 1 and 2σ marginalized probability regions obtained assuming constant γ and w (red solid curves) or assuming the parameterizations (6) and (4) and marginalizing over γ_1 and w_1 (black dashed curves); marginalized error values are in columns $\sigma_{\gamma_{\rm marg,1}}$, $\sigma_{w_{\rm marg,1}}$ of Tab. IX. Yellow dots represent the fiducial model, the triangles a $f(R)$ model and the squares mark the flat DGP.

The results obtained this Section can be summarized as follows.

1. If both γ and w are assumed to be constant and setting $\Omega_k = 0$ then, a redshift survey described by our *Reference case* will be able to constrain these parameters to within 4% and 2%, respectively.

2. Marginalizing over Ω_k degrades these constraints to 5.5% and 4% respectively.

3. If w and γ are considered redshift-dependent and parametrized according to eqs (6) and (4) then the errors on γ_0 and w_0 obtained after marginalizing over γ_1 and w_1 increase by a factor $\sim 4, 5$, i.e. we expect to measure γ_0 and w_0 with a precision of 13-15% and 11-14% respectively, where the interval reflects the uncertainties in the characteristic of the survey. With this precision we will be able to distinguish the fiducial model from the DGP and $f(R)$ scenarios with more than 2σ significance.

bias	case	σ_γ	σ_w	FOM
$b=\sqrt{1+z}$	ref.	0.03	0.04	1179
	opt.	0.03	0.03	1568
	pess.	0.04	0.05	706

Table VII: Numerical values for 1σ constraints on parameters γ and w (no parameterization), relative to the red ellipses in Figs 5, 8 and figures of merit. Here we have marginalized over Ω_k.

	case	σ_h	$\sigma_{\Omega_m h^2}$	$\sigma_{\Omega_b h^2}$	σ_{Ω_k}	σ_{n_s}
$b=\sqrt{1+z}$	ref.	0.024	0.008	0.002	0.01	0.02

Table VIII: Numerical values for marginalized 1σ constraints on Cosmological parameters using constant γ and w.

4. The ability to discriminate these models with a significance above 2σ is confirmed by the confidence contours drawn in the γ_0-γ_1 plane, obtained after marginalizing over all other parameters.

5. If we allow for a coupling between dark matter and dark energy, and we marginalize over η rather than over γ_1, then the errors on γ_0 and w_0 are almost identical to those obtained in the case of the γ-*parameterization*. However, our ability in separating the fiducial model from the CDE model is significantly hampered: the confidence contours plotted in the γ-η plane show that discrimination can only be performed wit 1-1.5σ significance.

VI. CONCLUSIONS

In this paper we addressed the problem of determining the growth rate of density fluctuations from the estimate of the galaxy power spectrum at different epochs in future redshift survey. As a reference case we have considered the proposed EUCLID spectroscopic survey modeled according to the latest, publicly available survey characteristics [26, 65]. In this work we focused on a few issues that we regard as very relevant and that were not treated in previous, analogous Fisher Matrix analysis mainly aimed at optimizing the survey setup and the observational strategy. These issues are: *i*) the ability in measuring self-consistently galaxy bias with no external information and the impact of treating the bias as an extra free parameter on the error budget; *ii*) the impact of choosing a particular parameterization in determining the growth rate and in distinguishing dark energy models with very different physical origins (in particular we focus on the ΛCDM, $f(R)$ and the DGP, models that are still degenerate with respect to present growth rate data); *iii*) the estimate of how errors on the growth rate depend on the degrees of freedom in the Fisher matrix analysis; *iv*) the ability of estimating a possible coupling between dark matter and dark energy.

The main results of the analysis were already listed in the previous Section, here we recall the most relevant ones.

1. With the "internal bias" method we were able to estimate bias with 1% accuracy in a self consistent way using only galaxy positions in redshift-space. The precision in measuring the bias has a very little dependence on the functional form assumed for $b(z)$. Measuring b with 1% accuracy will be a remarkable result also from an astrophysical point of view, since it will provide a strong, indirect constraint on the models of galaxy evolution.

bias	case	$\sigma_{\gamma_{marg,1}}$	$\sigma_{w_{marg,1}}$	FOM	$\sigma_{\gamma_{marg,2}}$	$\sigma_{w_{marg,2}}$	FOM
$b=\sqrt{1+z}$	ref.	0.08	0.11	241.1	0.09	0.11	104.1
	opt.	0.07	0.09	323.5	0.07	0.09	138.2
	pess.	0.11	0.14	142.5	0.11	0.15	61.6

Table IX: 1σ marginalized errors for parameters γ and w expressed through γ and η parameterizations. Columns $\gamma_{0,marg1}, w_{0,marg1}$ refer to marginalization over γ_1, w_1 (Fig. 5) while columns $\gamma_{0,marg2}, w_{0,marg2}$ refer to marginalization over η, w_1 (Fig. 8).

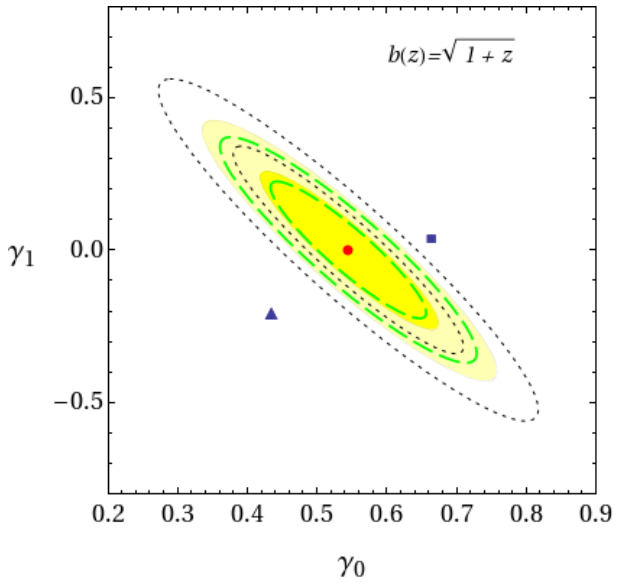

Figure 6: γ-parameterization. 1 and 2σ marginalized probability regions for the parameters γ_0 and γ_1, relative to the *Reference case* (shaded yellow regions), to the *Optimistic case* (green long-dashed ellipses), and to the *Pessimistic case* (black dotted ellipses). Red dots represent the fiducial model, blue squares mark the DGP while triangles stand for the $f(R)$ model. Then, in the case of γ-parameterization, one could distinguish these three models (at 95% probability).

bias	case	σ_{γ_0}	σ_{γ_1}	FOM
$b=\sqrt{1+z}$	ref.	0.08	0.17	178.4
	opt.	0.07	0.15	227.5
	pess.	0.11	0.22	112.4

Table X: Numerical values for 1σ constraints on parameters in Fig. 6 and figures of merit.

2. We have demonstrated that measuring the amplitude and the slope of the power spectrum in different z-bin allows to constrain the growth rate with good accuracy, with no need to assume an external error for $b(z)$. In particular, we found that s can be constrained at 1σ to within 3% in each of the 8 redshift bin from $z=0.5$ to 2.1. This result is robust to the choice of the biasing function $b(z)$. The accuracy in the measured s will be good enough to discriminate among the most popular competing models of dark energy and modified gravity.

3. Taking into account the possibility of a coupling between dark matter and dark energy has the effect of loosening the constraints on the relevant parameters, decreasing the statistical significance in distinguishing models (from $\gtrsim 2\sigma$ to $\lesssim 1.5\sigma$). Yet, this is still a remarkable improvement over the present situation, as can be appreciated from Fig. 9 where we compare the constraints expected by next generation data to the present ones. Moreover, the *Reference* survey will be able to constrain the parameter η to within 0.04. Reminding that we can write $\eta = 2.1\beta_c^2$ [4], this means that the coupling parameter β_c between dark energy and dark matter can be constrained to within 0.14, solely employing the growth rate information. This is comparable to existing constraints from the CMB but is complementary since obviously it is obtained at much smaller redshifts. A variable

bias	case	σ_γ	σ_η	FOM
$b=\sqrt{1+z}$	ref.	0.08	0.04	464.1
	opt.	0.07	0.03	608.2
	pess.	0.11	0.05	280.3

Table XI: Numerical values for 1σ constraints on parameters in Fig. 9 and figures of merit.

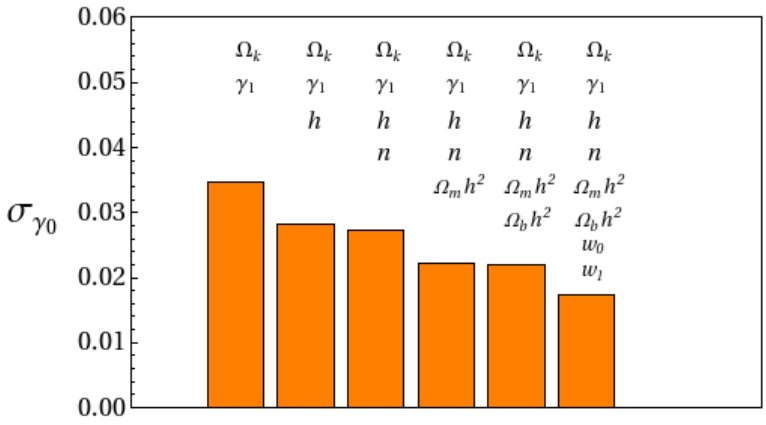

Figure 7: The bars represent the errors on the growth index γ_0 obtained using the γ-*parameterization* and fixing an increasing number of cosmological parameters as indicated over each bar and marginalizing over the others. The progressive increase in the number of fixed parameters reflects in a decrease of the error.

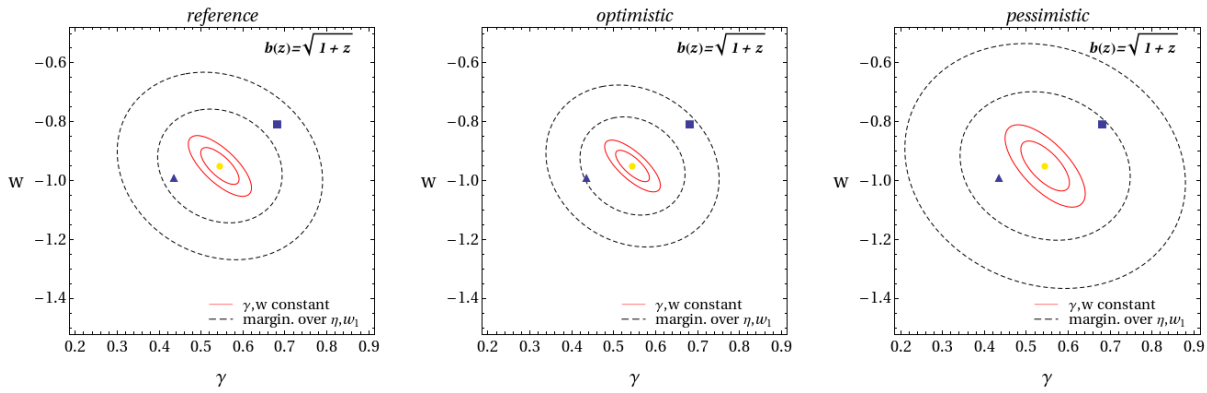

Figure 8: η-parameterization. 1 and 2σ marginalized probability regions obtained assuming constant γ and w (red solid curves) or assuming the parameterizations (7) and (4) and marginalizing over η and w_1 (black dashed curves); marginalized error values are in columns $\sigma_{\gamma_{\rm marg,2}}$, $\sigma_{w_{\rm marg,2}}$ of Tab. X. Yellow dots represent the fiducial model, the triangles stand for a $f(R)$ model and the squares mark the flat DGP.

coupling could therefore be detected by comparing the redshift survey results with the CMB ones.

It is worth pointing out that, whenever we have performed statistical tests similar to those already discussed by other authors in the context of a EUCLID-like survey, we did find consistent results. Examples of this are the values of FOM and errors for w_0, w_1, similar to those in [37, 40] and the errors on constant γ and w [40]. However, let us notice that all these values strictly depend on the parameterizations adopted and on the numbers of parameters fixed or marginalized over. In particular, we also found that all these constraints can be improved if one uses additional information from e.g. CMB and other observations.

	σ_{w_0}	σ_{w_1}	FOM
γ_0, γ_1 fixed	0.04	0.24	166
Ω_k fixed and marginalization over both γ_0, γ_1	0.12	0.36	97.3
marginalization over all other parameters	0.12	0.43	41.3

Table XII: 1 σ marginalized errors for the parameters w_0 and w_1, obtained with three different methods (reference case, see Fig. 10).

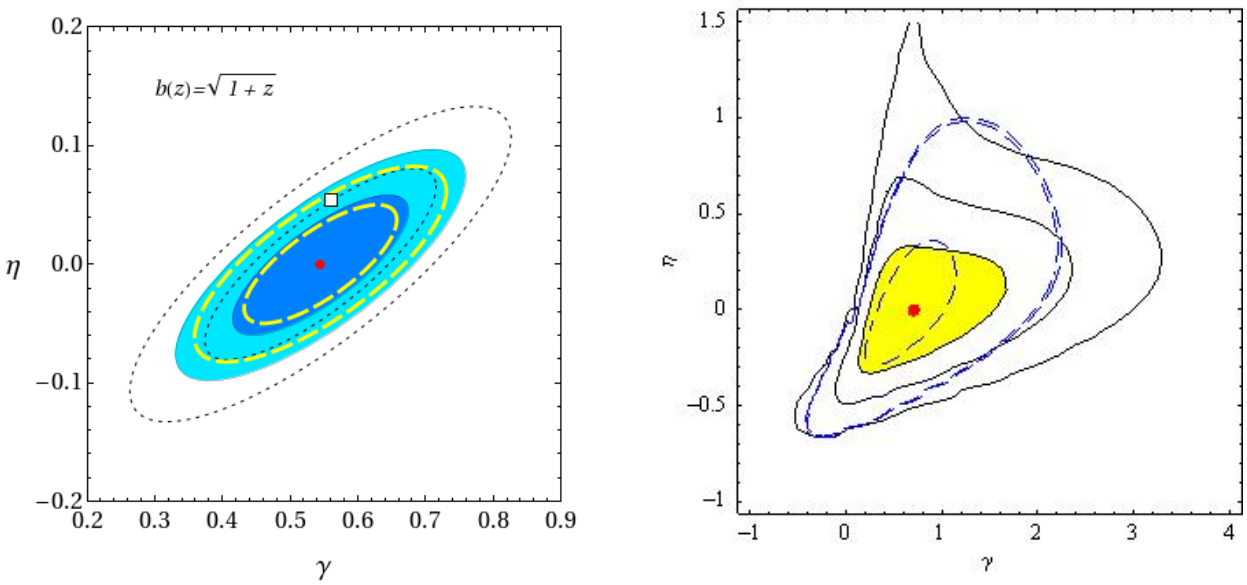

Figure 9: η-parameterization. Left panel: 1 and 2σ marginalized probability regions for the parameters γ and η in eq. (7) relative to the reference case (shaded blue regions), to the optimistic case (yellow long-dashed ellipses) and to the pessimistic case (black short-dashed ellipses). The red dot marks the fiducial model while the square represents the coupling model. Right panel: present constraints on γ and η computed through a full likelihood method (here the red dot marks the likelihood peak) [4]; long-dashed contours are obtained assuming a prior for $\Omega_{m,0}$.

We made a first step in this direction in Fig. (7), which shows how the errors on a constant γ decrease when progressively more parameters are fixed by external priors.

Acknowledgements

This work is supported by the DFG through TRR33 "The Dark Universe". We wish to thank Gigi Guzzo and Andrea Cimatti for insightful suggestions on an earlier draft of this paper.

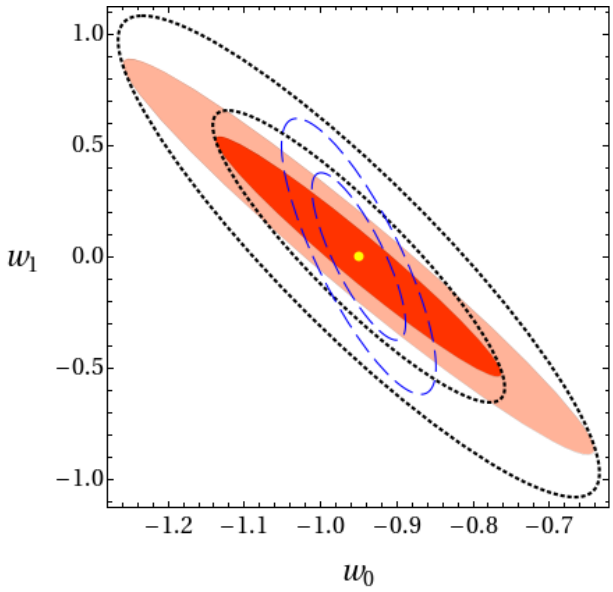

Figure 10: Errors on the equation of state. 1 and 2σ marginalized probability regions for the parameters w_0 and w_1, relative to the reference case and constant bias $b = 1$. The blue dashed ellipses are obtained fixing γ_0, γ_1 to their fiducial values and marginalizing over all the other parameters; for the red shaded ellipses instead, we also marginalize over γ_0, γ_1 but we fix $\Omega_k = 0$. Finally, the black dotted ellipses are obtained marginalizing over all parameters but w_0 and w_1. The progressive increase in the number of parameters reflects in a widening of the ellipses with a consequent decrease in the figures of merit (see Tab. XII).

[1] A. De Felice and S. Tsujikawa, "f(R) theories", *Living Rev.Rel.* **13** (2010) 3, arXiv:1002.4928 [gr-qc].

[2] G. Dvali, G. Gabadadze, and M. Porrati, "4-D gravity on a brane in 5-D Minkowski space", *Phys.Lett.* **B485** (2000) 208–214, arXiv:hep-th/0005016 [hep-th].

[3] Y. Wang, "Differentiating dark energy and modified gravity with galaxy redshift surveys", *JCAP* **0805** (2008) 021, arXiv:0710.3885 [astro-ph].

[4] C. Di Porto and L. Amendola, "Observational constraints on the linear fluctuation growth rate", *Phys.Rev.* **D77** (2008) 083508, arXiv:0707.2686 [astro-ph].

[5] R. Gannouji, B. Moraes, and D. Polarski, "The growth of matter perturbations in $f(R)$ models", *JCAP* **0902** (2009) 034, arXiv:0809.3374 [astro-ph].

[6] S. Tsujikawa, R. Gannouji, B. Moraes, and D. Polarski, "The dispersion of growth of matter perturbations in $f(R)$ gravity", *Phys.Rev.* **D80** (2009) 084044, arXiv:0908.2669 [astro-ph.CO].

[7] L. L. Amendola and T. S., *Dark energy Theory and Observations*. Cambridge University Press, 2010.

[8] A. Hamilton, "Linear redshift distortions: A Review", arXiv:astro-ph/9708102 [astro-ph]. Published in The Evolving Universe. Edited by D. Hamilton, Kluwer Academic, 1998, p. 185-275.

[9] H.-J. Seo and D. J. Eisenstein, "Probing dark energy with baryonic acoustic oscillations from future large galaxy redshift surveys", *Astrophys.J.* **598** (2003) 720–740, arXiv:astro-ph/0307460 [astro-ph].

[10] L. Amendola, C. Quercellini, and E. Giallongo, "Constraints on perfect fluid and scalar field dark energy models from future redshift surveys", *Mon.Not.Roy.Astron.Soc.* **357** (2005) 429–439, arXiv:astro-ph/0404599 [astro-ph].

[11] D. Sapone and L. Amendola, "Constraining the growth factor with baryon oscillations", arXiv:0709.2792 [astro-ph].

[12] L. Guzzo, M. Pierleoni, B. Meneux, E. Branchini, O. Fevre, *et al.*, "A test of the nature of cosmic acceleration using galaxy redshift distortions", *Nature* **451** (2008) 541–545, arXiv:0802.1944 [astro-ph].

[13] C. Blake, S. Brough, M. Colless, W. Couch, S. Croom, *et al.*, "The WiggleZ Dark Energy Survey: the selection function and z=0.6 galaxy power spectrum", *Mon.Not.Roy.Astron.Soc.* **406** (2010) 803–821, arXiv:1003.5721 [astro-ph.CO].

[14] J. da Angela, T. Shanks, S. Croom, P. Weilbacher, R. Brunner, *et al.*, "The 2dF-SDSS LRG and QSO Survey: QSO clustering and the $L-z$ degeneracy", *Mon.Not.Roy.Astron.Soc.* **383** (2008) 565–580, arXiv:astro-ph/0612401 [astro-ph].

[15] E. Hawkins, S. Maddox, S. Cole, D. Madgwick, P. Norberg, *et al.*, "The 2dF Galaxy Redshift Survey: Correlation functions, peculiar velocities and the matter density of the universe", *Mon.Not.Roy.Astron.Soc.* **346** (2003) 78, arXiv:astro-ph/0212375 [astro-ph].

[16] J. A. Peacock, S. Cole, P. Norberg, C. M. Baugh, J. Bland-Hawthorn, *et al.*, "A Measurement of the cosmological mass density from clustering in the 2dF Galaxy Redshift Survey", *Nature* **410** (2001) 169–173, arXiv:astro-ph/0103143 [astro-ph].

[17] N. P. Ross, J. da Angela, T. Shanks, D. A. Wake, R. D. Cannon, *et al.*, "The 2dF-SDSS LRG and QSO Survey: The 2-Point Correlation Function and Redshift-Space Distortions", *Mon.Not.Roy.Astron.Soc.* **381** (2007) 573–588, arXiv:astro-ph/0612400 [astro-ph].

[18] **SDSS Collaboration** Collaboration, M. Tegmark *et al.*, "Cosmological Constraints from the SDSS Luminous Red Galaxies", *Phys.Rev.* **D74** (2006) 123507, arXiv:astro-ph/0608632 [astro-ph].

[19] L. Verde, A. F. Heavens, W. J. Percival, S. Matarrese, C. M. Baugh, *et al.*, "The 2dF Galaxy Redshift Survey: The Bias of galaxies and the density of the Universe", *Mon.Not.Roy.Astron.Soc.* **335** (2002) 432, arXiv:astro-ph/0112161 [astro-ph].

[20] **SDSS Collaboration** Collaboration, P. McDonald *et al.*, "The Linear theory power spectrum from the Lyman-α forest in the Sloan Digital Sky Survey", *Astrophys.J.* **635** (2005) 761–783, arXiv:astro-ph/0407377 [astro-ph].

[21] A. Nusser and M. Davis, "The cosmological bulk flow: consistency with ΛCDM and $z \approx 0$ constraints on σ_8 and γ", arXiv:1101.1650 [astro-ph.CO].

[22] J. Dossett, M. Ishak, J. Moldenhauer, Y. Gong, and A. Wang, "Constraints on growth index parameters from current and future observations", *JCAP* **1004** (2010) 022, arXiv:1004.3086 [astro-ph.CO].

[23] S. Nesseris and L. Perivolaropoulos, "Testing ΛCDM with the Growth Function $\delta(a)$: Current Constraints", *Phys.Rev.* **D77** (2008) 023504, arXiv:0710.1092 [astro-ph].

[24] L. Guzzo and O. Le Fèvre, "Redshift-space distortions in deep redshift surveys as a probe of the invisible Universe", in *INVISIBLE UNIVERSE: Proceedings of the Conference*, vol. 1241 of *American Institute of Physics Conference Series*, pp. 39–45. June, 2010.

[25] D. Schlegel, M. White, and D. Eisenstein, "The Baryon Oscillation Spectroscopic Survey: Precision measurements of the absolute cosmic distance scale", arXiv:0902.4680 [astro-ph.CO].

[26] R. Laureijs *et al.*, "Euclid Assessment Study Report for the ESA Cosmic Visions", arXiv:0912.0914 [astro-ph.CO].

[27] D. J. Schlegel, C. Bebek, H. Heetderks, S. Ho, M. Lampton, *et al.*, "BigBOSS: The Ground-Based Stage IV Dark Energy Experiment", arXiv:0904.0468 [astro-ph.CO].

[28] O. Lahav *et al.*, "Dynamical effects of the cosmological constant", *Mon.Not.Roy.Astron.Soc.* **251** (1991) 128–136.

[29] E. V. Linder, "Cosmic growth history and expansion history", *Phys.Rev.* **D72** (2005) 043529, arXiv:astro-ph/0507263 [astro-ph].

[30] P. J. E. Peebles., "The Peculiar Velocity Field in the Local Supercluster", *Astrophys.J.* **205** (1976) 318–328.

[31] D. Polarski and R. Gannouji, "On the growth of linear perturbations", *Phys.Lett.* **B660** (2008) 439–443, arXiv:0710.1510 [astro-ph].

[32] L.-M. Wang and P. J. Steinhardt, "Cluster abundance constraints on quintessence models", *Astrophys.J.* **508** (1998) 483–490, arXiv:astro-ph/9804015 [astro-ph].

[33] E. V. Linder and R. N. Cahn, "Parameterized Beyond-Einstein Growth", *Astropart.Phys.* **28** (2007) 481–488, arXiv:astro-ph/0701317 [astro-ph].

[34] H. Wei, "Growth Index of DGP Model and Current Growth Rate Data", *Phys.Lett.* **B664** (2008) 1–6, arXiv:0802.4122 [astro-ph].

[35] C. Marinoni, O. Le Fèvre, B. Meneux, A. Iovino, A. Pollo, *et al.*, "The VIMOS VLT Deep Survey: Evolution of the non-linear galaxy bias up to z=1.5", *Astron.Astrophys.* **442** (2005) 801–825, arXiv:astro-ph/0506561 [astro-ph].

[36] Y. Sigad, E. Branchini, and A. Dekel, "Measuring the nonlinear biasing function from a galaxy redshift survey", *Astrophys.J.* **540** (2000) 62–73, arXiv:astro-ph/0002170 [astro-ph].

[37] Y. Wang, W. Percival, A. Cimatti, P. Mukherjee, L. Guzzo, *et al.*, "Designing a space-based galaxy redshift survey to probe dark energy", *Mon.Not.Roy.Astron.Soc.* **409** (2010) 737–749, arXiv:1006.3517 [astro-ph.CO].

[38] F. Simpson and J. A. Peacock, "Difficulties Distinguishing Dark Energy from Modified Gravity via Redshift Distortions", *Phys.Rev.* **D81** (2010) 043512, arXiv:0910.3834 [astro-ph.CO].

[39] L. Samushia, W. J. Percival, L. Guzzo, Y. Wang, A. Cimatti, *et al.*, "Effects of cosmological model assumptions on galaxy redshift survey measurements", *Mon.Not.Roy.Astron.Soc.* (2010) in press, arXiv:1006.0609 [astro-ph.CO].

[40] E. Majerotto *et al. in preparation* .

[41] M. Chevallier and D. Polarski, "Accelerating universes with scaling dark matter", *Int.J.Mod.Phys.* **D10** (2001) 213–224, arXiv:gr-qc/0009008 [gr-qc].

[42] E. V. Linder, "Exploring the expansion history of the universe", *Phys.Rev.Lett.* **90** (2003) 091301, arXiv:astro-ph/0208512 [astro-ph].

[43] X.-y. Fu, P.-x. Wu, and H.-w. Yu, "The Growth of linear perturbations in the DGP model", *Phys.Lett.* **B677** (2009) 12–15, arXiv:0905.1735 [gr-qc].

[44] P. Wu, H. W. Yu, and X. Fu, "A Parametrization for the growth index of linear matter perturbations", *JCAP* **0906** (2009) 019, arXiv:0905.3444 [gr-qc].

[45] H. Motohashi, A. A. Starobinsky, and J. Yokoyama, "Phantom behaviour and growth index anomalous evolution in viable $f(R)$ gravity models", arXiv:1002.0462 [astro-ph.CO].

[46] A. Dekel and O. Lahav, "Stochastic nonlinear galaxy biasing", *Astrophys.J.* **520** (1999) 24–34, arXiv:astro-ph/9806193 [astro-ph].

[47] K. Kovac, C. Porciani, S. Lilly, C. Marinoni, L. Guzzo, *et al.*, "The nonlinear biasing of the 10k zCOSMOS galaxies up to $z \sim 1$", arXiv:0910.0004 [astro-ph.CO].

[48] A. Rassat, A. Amara, L. Amendola, F. J. Castander, T. Kitching, *et al.*, "Deconstructing Baryon Acoustic Oscillations: A Comparison of Methods", arXiv:0810.0003 [astro-ph].

[49] A. Orsi, C. Baugh, C. Lacey, A. Cimatti, Y. Wang, *et al.*, "Probing dark energy with future redshift surveys: A comparison of emission line and broad band selection in the near infrared", *Mon.Not.Roy.Astron.Soc.* **405** (2010) 1006–1024, arXiv:0911.0669 [astro-ph.CO].

[50] C. M. Baugh, C. Lacey, C. Frenk, G. Granato, L. Silva, *et al.*, "Can the faint submillimetre galaxies be explained in the Λ cold dark matter model?", *Mon.Not.Roy.Astron.Soc.* **356** (2005) 1191–1200, arXiv:astro-ph/0406069 [astro-ph].

[51] A. Albrecht, G. Bernstein, R. Cahn, W. L. Freedman, J. Hewitt, *et al.*, "Report of the Dark Energy Task Force", arXiv:astro-ph/0609591 [astro-ph].

[52] R. Maartens and E. Majerotto, "Observational constraints on self-accelerating cosmology", *Phys.Rev.* **D74** (2006) 023004, arXiv:astro-ph/0603353 [astro-ph].

[53] W. Hu and I. Sawicki, "Models of $f(R)$ Cosmic Acceleration that Evade Solar-System Tests", *Phys.Rev.* **D76** (2007) 064004, arXiv:0705.1158 [astro-ph].

[54] L. Amendola, "Coupled quintessence", *Phys.Rev.* **D62** (2000) 043511, arXiv:astro-ph/9908023 [astro-ph].

[55] C. Wetterich, "The Cosmon model for an asymptotically vanishing time dependent cosmological 'constant'", *Astron.Astrophys.* **301** (1995) 321–328, arXiv:hep-th/9408025 [hep-th].

[56] L. Amendola and C. Quercellini, "Tracking and coupled dark energy as seen by WMAP", *Phys.Rev.* **D68**

(2003) 023514, arXiv:astro-ph/0303228 [astro-ph].
[57] R. A. Fisher, "The logic of inductive inference", *J. Roy. Stat. Soc.* **98** (1935) 39–54.
[58] M. Tegmark, A. Taylor, and A. Heavens, "Karhunen-Loéve eigenvalue problems in cosmology: How should we tackle large data sets?", *Astrophys.J.* **480** (1997) 22, arXiv:astro-ph/9603021 [astro-ph].
[59] U. Seljak and M. Zaldarriaga, "A Line of sight integration approach to cosmic microwave background anisotropies", *Astrophys.J.* **469** (1996) 437–444, arXiv:astro-ph/9603033 [astro-ph].
[60] N. Kaiser, "Clustering in real space and in redshift space", *Mon.Not.Roy.Astron.Soc.* **227** (1987) 1–21.
[61] D. J. Eisenstein, H.-j. Seo, and . White, Martin J., "On the Robustness of the Acoustic Scale in the Low-Redshift Clustering of Matter", *Astrophys.J.* **664** (2007) 660–674, arXiv:astro-ph/0604361 [astro-ph].
[62] H.-J. Seo and D. J. Eisenstein, "Improved forecasts for the baryon acoustic oscillations and cosmological distance scale", *Astrophys.J.* **665** (2007) 14–24, arXiv:astro-ph/0701079 [astro-ph].
[63] E. Komatsu, K. Smith, J. Dunkley, C. Bennett, B. Gold, *et al.*, "Seven-Year Wilkinson Microwave Anisotropy Probe (WMAP) Observations: Cosmological Interpretation", arXiv:1001.4538 [astro-ph.CO].
[64] M. Tegmark, "Measuring cosmological parameters with galaxy surveys", *Phys.Rev.Lett.* **79** (1997) 3806–3809, arXiv:astro-ph/9706198 [astro-ph].
[65] J. Geach, A. Cimatti, W. Percival, Y. Wang, L. Guzzo, *et al.*, "Empirical Hα emitter count predictions for dark energy surveys", *Mon.Not.Roy.Astron.Soc.* **402** (2010) 1330–1338, arXiv:0911.0686 [astro-ph.CO].